# Conceptual Design Analysis for a Two-Stage-to-Orbit Semi-Reusable Launch System for Small Satellites

Christie Alisa Maddock*, Lorenzo Ricciardi

*Aerospace Centre of Excellence, University of Strathclyde, Glasgow, United Kingdom*

Michael West, Joanne West

*BAE Systems Regional Aircraft, Prestwick, United Kingdom*

Konstantinos Kontis, Sriram Rengarajan

*Aerospace Sciences, University of Glasgow, Glasgow, United Kingdom*

David Evans, Andy Milne

*Fluid Gravity Engineering, Hants, United Kingdom*

Stuart McIntyre

*Orbital Access, Prestwick, United Kingdom*

---

**Abstract**

This paper presents the conceptual design and performance analysis of a partially reusable space launch vehicle for small payloads. The system employs a multi-stage vehicle powered by rocket engines, with a reusable first stage capable of glided or powered flight, and expendable upper stage(s) to inject 500 kg of payload into low Earth orbits. The space access vehicle is designed to be air-launched from a modified aircraft carrier. The aim of the system design is to develop a commercially viable launch system for near-term operation, thus emphasis is placed on the efficient use of high TRL technologies and on the commercial potential of the technical design. The vehicle design

*Corresponding author

*Email addresses:* christie.maddock@strath.ac.uk (Christie Alisa Maddock), michael.west@baesystems.com (Michael West), kostas.kontis@glasgow.ac.uk (Konstantinos Kontis), david.evans@fluidgravity.co.uk (David Evans), smcintyre@orbital-access.com (Stuart McIntyre)

is analysed using a multi-disciplinary design optimisation approach to evaluate the performance, operational capabilities and design trade-offs. Results from two trade-off studies are shown, evaluating the choice wing area and thus aerodynamic characteristics, and the choice of stage masses and engines selection on the mission performance.

*Keywords:* space access, trajectory optimisation, space transportation

---

## 1. Introduction

The space market is shifting to include smaller satellites with a focus on expanding commercial applications. Since 2012, 71% of satellites launched have a spacecraft mass less than 600 kg, with 34% of those being cubesats (Maddock et al., 2016a). The growing market for downsteam applications from single consumers to large businesses, and the planned development of mega-constellations has translated into a predicted demand for small satellite launchers, from a current launch rate of 400 satellites in 2016, to a forecasted market of 600 by 2020, and over 2000 satellites by 2030 (Maddock et al., 2016a).

Along with this predicted growth, is a predicted bottleneck due to low-cost launch options. A forecast by SpaceWorks overestimated the number of nano/microsatellites launched in 2016 by nearly 100%, predicting 210 satellites launched compared to an actual figure of only 101. Their forecast for 2017 predicts a continuing high backlog of nano- and microsats due to "technical challenges and limited launch vehicle availability." (Doncaster et al., 2017)

These commercial drivers within the *new space* (Hay et al., 2009) market have also driven a number of government initiatives, in particular in the domain of space access. The UK National Space Policy (2016) states "access to safe and cost-effective launchers is clearly fundamental to any countrys long term capacity to participate in space-based activities." There have been a number of programmes to establish a UK-based operational spaceport, and to promote the UK commercial space sector within the global market.

Orbital Access formed to lead the development of UK small payload launch systems and provide launch services from the UK and globally. The goal is to develop commercially viable launch systems tailored to meet the needs of UK payload manufacturers and secure the IPR and industrial value in the UK manufacturing base. In 2015, Orbital Access formed a consortium

with several aerospace companies, research centres and universities to further advance the UK space access sector, in particular to develop national technology roadmaps, market forecast studies (Maddock et al., 2016a), technical studies and R&D ventures under the Future UK Small Payload Launcher ($FSPL^{UK}$) programme.

Several industrial research projects have been carried out towards the conceptual design of a of a two-stage to orbit, semi-reusable launch system for small satellites. The aim of the system design is to develop a commercially viable launch system for near-term operation, thus emphasis is placed on the efficient use of high TRL technologies. The commercial viability is the underlying driver for all the mission and system requirements during the initial stages of design.

The following details the progress made on the conceptual design and analysis focusing on concept feasibility. A multidisciplinary design optimisation was undertaken to assess key design parameters within the vehicle design. The vehicle sizing and performance was optimised against a set of mission requirements stemming from the commercial drivers.

The system is a multi-stage vehicle using rocket propulsion that will be air-launched from a carrier aircraft. The main vehicle is a reusable spaceplane design allowing for unpowered, glided re-entry/return flights. The second stage(s) are stored within the main body of the spaceplane, among other benefits this allows for better control of the moments induced by the movement of the centre of gravity though introduces complexity and release issues. The main operational spaceport is located at Prestwick on the western coast of Scotland, with alternate landing sites identified in Northern Europe and Scandinavia. The air-launch increases the range of orbits that can be reached, and improves the flexibility of the system by allowing the transport and recovery of the first stage.

In particular, the paper describes the overall approach with design objectives and mission requirements, then details the subsystem models developed for use within a specialised integrated design platform for space access vehicles. The optimisation used within the system performance analysis is described, with results presented examining the trade-off in performance of altering key design variables in the configuration, specifically the engine and wing sizing (aerodynamic efficiency). The nominal mission is to deploy 500 kg payload into 650 km altitude circular orbit at an inclination of 88.2 deg, targeting the OneWeb constellation. An extended mission would deploy 150 kg payload, equivalent to a single OneWeb satellite, to a 1200 km altitude,

circular polar low earth orbit in the same inclination plane.

## 2. Approach

The design approach for the concept feasibility phase is to assess the design drivers linking the commercially-driven mission and system requirements to technical design parameters.

A previous study by Maddock et al. (2016a,b) looked at a market forecast and demand study and developed a cost model relating the technology readiness level (TRL) of critical technologies to the development cost against the predicted market demands. The output drove to the design decisions, mapped into requirements, for a reusable first stage based on COTS (TRL 8-9) rocket engines. The decision to air-launch the vehicle from modified commercial carrier aircraft will allow the system to operate globally and increases the flexibility of the system to reach different orbits, and have different take-off and landing sites. Based on an evaluation of the TRL, and impact on cost, of certain technologies, a number of additional constraints were determined, for example the acceleration limits and heating loads.

The launch vehicle is modelled in a modular format to be run within a multi-disciplinary design optimisation (MDO) environment. The MDO software can optimise the performance of the system by adjusting a number of optimisation control parameters. Computationally fast engineering models were developed for the different subsystems of the vehicle, and the operational environment.

Different design criteria were selected as inputs with the models relating the impact of changes on those variables on the system. In this study, three design variables are analysed to size the wing area and engine sizing of the first and second stage. The aerodynamic wing reference area affects the aerodynamic performance, generating necessary lift for the glide re-entry while minimising drag on the ascent, and the vehicle dry mass. The performance of the engines affect the maximum level of thrust produced, the vehicle dry mass and impacts the fuel mass required. The trajectory for both ascent and descent is simultaneously optimised to minimise the mass of the required on-board propellant and oxidiser.

The mission is analysed in a single optimisation, starting just after the spaceplane is released from carrier aircraft and includes the Stage 1 ascent and descent to an spaceport approach, and the Stage 2 ascent and injection into orbit.

## 3. System models

In this section, mathematical models are presented for the vehicle design and operation. The models are divided by discipline: vehicle mass and configuration, aerodynamics, propulsion, environment models for Earth including geometry, gravitational field and atmospheric model, and the flight dynamics and control.

### *3.1. Vehicle configuration*

The fundamental systems concept consists of a winged recoverable booster vehicle which is air launched from a converted large commercial aircraft. The booster carries one or multiple disposable upper stages, each with their own individual payload. The vehicle configuration is driven by the constraints inherent in an air launched system and the desire to provide as much flexibility as possible in the payload carriage.

An earlier study (Maddock et al., 2017) describes the evolution of the concept from a winged rocket to an integrated spaceplane with a central payload cartridge. This concept allows for rapid integration of payloads and associated upper stages into the booster, the payload cartridges themselves being loaded and integration tested remotely. This allows each booster to attain the high launch rates required for an economically attractive business case.

The following analysis is for a ventral launch system, wherein the booster is mounted under a converted large commercial aircraft. For the purposes of the study in question, this was taken to be a McDonnell Douglas DC-10 / MD-11 series aircraft, which has significant advantages in terms of underfuselage space volume over other types. The primary design constraints driven by this concept are the maximum height of the booster due to ground clearance and the maximum launch mass. In addition, the wing span of the booster is limited by clearance from the carrier aircraft wing-mounted engines and the length is fixed by the carrier aircraft nose gear and the tail strike angle.

A parametric mass estimation tool was developed based on a number of published methods for both reusable launch vehicles and high performance aircraft (Maddock et al., 2017; Rohrschneider, 2002; MacConochie and Lepsch Jr, 2002). Using this tool, full component mass breakdowns and scaling laws were determined and supplied to the trajectory analysis and sizing models. Mass estimating relationships were developed for the major structural

components (e.g., wing, fins, fuselage structure, propellant tanks) and major systems (e.g., propulsion, avionics, landing gear) to determine the gross and dry masses of the stages as a function of the optimisable design inputs.

To allow for resizing during the vehicle optimisation phase, parametric scaling equations of the form,

$$m_{new} = m_{ref} \left( \frac{S_{new}}{S_{ref}} \right)^{b} \tag{1}$$

were developed for the major components, where $m$ is the mass, $S$ is a reference value for the scalable component, and $b$ is a scaling exponent.

Knowing the mass breakdown and component layouts, the vehicle centre of gravity and its variation with fuel burn and payload deployment was determined and assessments made of the ability to trim i.e., reduce the pitching moment to zero during ascent and re-entry. Following this the propellant tanks were redistributed to give an acceptable centre of gravity range during flight. The internal layout of the configuration is shown in Fig. 1. Note that the propulsion system shown is indicative of the size and location but does not include any engineering details of the installation.

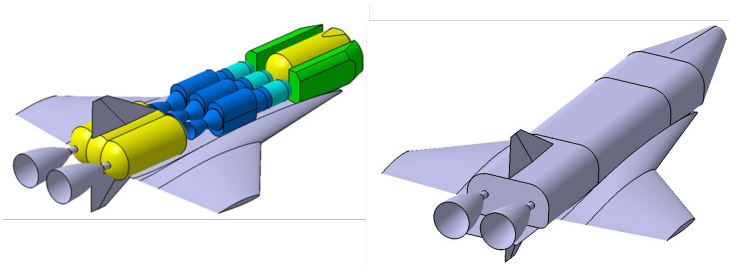

Figure 1: General configuration and internal layout

### *3.2. Aerodynamics*

The aerodynamic force coefficients for the vehicle configuration were estimated for Mach numbers ranging from 0.2 to 30, angles of attack of $-5°$ to $40°$ and for altitudes up to 100 km. The drag coefficient at zero incidence $C_{D_0}$ and the normal force coefficient $C_N$ at different angles of attack $\alpha$ for each component of the vehicle (fuselage, fairing, wings and tail) are estimated separately. The approach for the estimation is based on different theories for

each Mach number range, from subsonic to hypersonic, detailed by Mason et al. (1981) and Fleeman (2001).

The lift and drag force coefficients of each component at different Mach numbers and angles of attack are modelled by,

$$C_L = C_N \cos\alpha - C_{D_0} \sin\alpha \tag{2a}$$

$$C_D = C_N \sin\alpha + C_{D_0} \cos\alpha \tag{2b}$$

Eqs. 2 are applicable for small angles of attack at which the axial force is approximately equal to drag. Although large angles of attack are considered the method is expected over predict the lift at such angles. This is further complicated by the stall effects at higher angles, which are not accounted in the method. Through validation with experimental data Jorgensen (1973); Singh (1996), the extent of deviation of the predictions from the experiments was assessed. However, the method considers the effect of flow separation at the base of the fuselage. The fuselage cross section is approximated to be elliptic (with same area of cross section and major axis equal to half of the maximum width of the fuselage) in order to enable the application of theories. The lift and drag coefficients, after normalization using the wing surface area, are then added up to give the total lift and drag coefficient of the entire configuration. Linear theory and modified Newtonian theory are used to deduce the wave drag coefficient at zero incidence over slender circular/elliptic nose $C_{d0,wave,b}$, wave drag coefficient at zero incidence over the delta wing (as well as tail, which has similar form) $C_{d0,wave,w}$, and the normal force coefficient as a function of angle of attack for the cone-cylinder $C_{N,b}$ as well as wings $C_{N,w}$, given by the following equations.

$$C_{d0,wave,b} = \begin{cases} 0 & \text{for } M < 1 \\ \frac{3.6 d_N}{\ell_N (M-1)+3} & \text{for } M \geq 1 \end{cases} \tag{3}$$

$$C_{d0,wave,w} = \begin{cases} 0 & \text{for } M < 1 \\ f\left(M_{\lambda LE}, \gamma, \delta_{LE}, tb/S_w\right) & \text{for } M \geq 1 \end{cases} \tag{4}$$

$$|C_{N,b}| = \frac{a_N}{b_N} \sin(2\alpha) \cos(\alpha/2) + 2\frac{\ell_C}{d_C} \tag{5}$$

$$|C_{N,w}| = \begin{cases} \frac{\pi A}{2} |\sin\alpha\cos\alpha| + 2\sin^2\alpha & \text{for } M^2 < 1 + (8/\pi A)^2 \\ \frac{4|\sin\alpha\cos\alpha|}{\sqrt{M^2-1}} + 2\sin^2\alpha & \text{for } M^2 \geq 1 + (8/\pi A)^2 \end{cases} \tag{6}$$

where $\ell_N$ is the length of the cone nose, $d_N$ is the equivalent diameter with major axis $a_N$ and minor axis $b_N$, $\ell_C$ is the length of the cylindrical body, $A$ is the aspect ratio of the wing, $t$ is the wing thickness, $b$ is the wing width, $S_w$ wing reference area, $\delta_{LE}$ is the wing thickness angle, $\gamma$ is the specific heat ratio, $\alpha$ is the angle of attack, and $M$ is the freestream Mach number with $M_{\lambda LE}$ the Mach number resolved in the direction normal to the wing leading edge with a sweep angle $\lambda_{LE}$.

The complex algebraic functional form $f$ of the base wave drag on the wing $C_{d0,wave,w}$ is given by Fleeman (2001). The above coefficients are all normalised by their respective reference areas (and not a common reference area).

The coast drag of the cone-cylinder body $C_{d0,c}$ is given by the following engineering correlation (Fleeman, 2001).

$$C_{d0,c} = \begin{cases} 0.12 + 0.13M^2 & \text{for } M < 1 \\ 0.25/M & \text{for } M \geq 1 \end{cases} \tag{7}$$

The inviscid drag at zero incidence also includes drag due to nose and leading edge bluntness, which are also estimated using the semi-empirical expressions given by Fleeman (2001).

While the inviscid coefficients are only dependent on Mach number and angle of attack and independent of altitude, the contribution of skin friction- which is dependent of Reynolds number- leads to altitude dependence of the force coefficients. The skin friction drag coefficient at zero incidence for the cone-cylinder body $C_{D0,f,b}$ and for the wing $C_{D0,f,w}$ (tail too has similar functional form) are given by the following engineering correlations.

$$C_{d0,f,b} = 0.053\frac{\ell}{d}\left(\frac{M}{q\ell}\right)^{0.2} \tag{8a}$$

$$C_{d0,f,w} = \frac{0.0266}{(qc_{max})^{0.2}} \tag{8b}$$

In the above equations $q$ is the dynamic pressure and $c_{max}$ is the length of mean wing chord. The skin friction drag coefficient is added to the inviscid drag coefficients at zero incidence (for each component). The lift and drag coefficients due to each component are then calculated using Eq. 2 from the estimated total drag coefficient at zero incidence and the normal force coefficient of the component.

The method is validated using wind tunnel data at Mach 2, 3 and 4 (Jorgensen, 1973) and using gun tunnel data at Mach 8.2 for a simple cone-cylinder configuration as well as a cone-cylinder with a pair of delta wings using gun-tunnel data (Singh, 1996). In general the comparison between the predictions and experiments were good up to an angle of attack of 10° after which the method starts to over-predict the lift, sometime by over 35%. This is because the wing stall is not presently considered. The drag for the wing configuration is also generally over-predicted, therefore giving a conservative estimate. Details of the validation, the comparison with the wind/gun tunnel data, and some illustrative results (predicted lift and drag coefficients) for the present aerodynamic configuration are presented by Maddock et al. (2017). The lift and drag coefficients for each individual components as well as for the whole vehicle configuration are thus estimated as a function of Mach number, angle of attack and altitude; thus the aerodynamic data of force coefficients is generated as three-dimensional arrays which, along with the aero-thermal models, is used in the subsequent analysis of flight trajectory and optimisation.

### *3.3. Aerothermodynamics*

An engineering level aerothermodynamics model is used to calculate indicative heat fluxes which can then be used to determine integrated heat loads and radiative equilibrium temperatures for the purpose of trajectory optimisation. This engineering model is in keeping with initial phase studies and the fidelity of aerodynamic models. The heat flux and equilibrium temperatures were determine for a fixed number of vehicle locations:

- nosetip stagnation point
- location of nosetip peak turbulent heating
- wing leading edge
- wing monitor point
- acreage monitor point

Indicative continuum laminar and turbulent heat transfer coefficients are calculated on the nosecone using the well-known formulation of Detra (1961) with the application of a suitable equivalent nose radius. This model is modified for the calculation of heat flux at a wing leading edge to take into

account the radius of curvature and sweep angle of the wing. The heat flux on the wing a given distance aft of the leading edge is calculated using a flat plate model with angle of attack effects. Acreage heat fluxes are calculated as a function of local surface inclination to the free-stream flow.

The laminar stagnation point heat flux $q_{st}$ is calculated using Detra and Hidalgos correlation (Detra, 1961),

$$q_{st} = 1.135\sqrt{\frac{\rho_\infty}{\rho_{ref}}}\left(\frac{865}{\sqrt{\frac{2R_n}{0.6096}}}\right)\left(\frac{v_\infty}{3048}\right)^{3.15} \tag{9}$$

where $R_n$ is the nose radius, $\rho_{ref}$ is a reference density defined as the density of air at sea level, and $\rho_\infty$ and $v_\infty$ are the free-stream density and velocity, respectively.

The peak turbulent heat flux on the nose cone is calculated assuming a hemispherical nose of radius $R_n$. The turbulent flux $q_t$ at a given point can be calculated using Detra and Hidalgo's turbulent correlation,

$$q_t = \frac{1.135}{\left(\frac{s}{0.3048}\right)^{0.2}}\left(\frac{\rho_\infty}{\rho_{ref}}\right)^{0.8}\left(\frac{v_\infty}{3048}\right)^{3.18}\phi_t \tag{10}$$

where $s$ is the stream length from the stagnation point to the point of interest and $\phi_t$ is a calibration factor accounting for the pressure distribution on the vehicle. Assuming a hemispherical nose and Newtonian pressure gradient allows for $s$ and $\phi_t$ corresponding to the location of peak turbulent heating on the nose to be calculated.

The corresponding laminar heat flux at the point of peak turbulent heat flux can be approximated by (SAE AC-9, 1969),

$$q_l = q_{st}\cos^{\frac{3}{2}}\gamma \tag{11}$$

where $\gamma$ is the angle from the nose centreline and the peak turbulent heat flux is then,

$$q_{tmax} = \max\left(q_t, q_l\right) \tag{12}$$

A simplified model for the heat flux at the wing leading edges, taking account of radius of curvature and sweep angle, is used (SAE AC-9, 1969). The wing leading edges are assumed to be exposed directly to the free stream to provide indicative fluxes. This condition is more likely to be satisfied

at higher Mach numbers but is also configuration and attitude dependent. Sweeping a wing or leading edge of a vehicle will generally result in a reduction in the convective heat flux at the surface.

An estimate of heating on the wings away from the leading edge or stagnation point is calculated using expressions. The wing is approximated as a flat plate at angle of attack $\alpha$ with the heat flux a distance from the leading edge based on the state of the boundary layer (SAE AC-9, 1969).

$$q_{w,x} = \begin{cases} q_{st}\left(x\right) \frac{0.0312}{1.068} \alpha^{\frac{2}{3}} & \text{for laminar} \\ q_{t}\left(x\right) \frac{0.333}{5.0} \alpha & \text{for turbulent} \end{cases} \tag{13}$$

where $q_{st}\left(x\right)$ is the Detra-Hidalgo equation for stagnation point heating in Eq. (9) evaluated at a nose radius of $x$. Similarly, $q_{t}\left(x\right)$ is the Detra-Hidalgo equation for peak turbulent heating in Eq. (10) evaluated at a nose radius of $x$. The resulting heating expressions for a wing monitor point are applicable far downstream from the leading edge (greater than approximately 10 leading edge radii from the leading edge). They can be used for preliminary analysis of aerodynamic heating but are not recommended for more detailed work.

It is not appropriate to approximate the acreage as a flat plate as is done for the wings. Instead, the heat flux at a point on the acreage $q_{acr}$ is calculated based on the modified Lees method,

$$q_{acr} = q_{st} k_1 \left(k_2 + \left(1 - k_2\right) \sin^{k_3} \theta\right) \tag{14}$$

where $\theta$ is the angle between the local surface and the free-stream flow and $k_1$, $k_2$ and $k_3$ are constants that must be calibrated. This expression is intended to be used for preliminary analysis. The constants are intended to be calibrated to higher fidelity predictions (boundary layer solutions for example) using the concept geometry. Hence, heat flux predictions can be easily adjusted through the three constants as the fidelity of future modelling increases.

Free molecular heating $q_{fm}$ is approximated in the limit of infinite speed ratio with complete thermal accommodation (which for the stagnation point is simply the incoming kinetic energy flux),

$$q_{fm} = \frac{1}{2} \rho_{\infty} v_{\infty}^{3} sin\theta \tag{15}$$

Accounting for the effects of finite speed ratio, varying thermal accommodation coefficient and varying temperature ratio (see e.g., Schaaf (1964)) can

easily be calculated, but would introduce a level of detail that is not justified at this stage of design.

For simplicity, the applied heat flux is taken to be the minimum selected from the continuum and free-molecular formulations at each point on the trajectory. This is justified for early design phase studies since it provides a conservative heat load when compared to more sophisticated Knudsen based bridging techniques. Hence, at any given trajectory point,

$$q = \min\left(q_{cont}, q_{fm}\right) \tag{16}$$

### *3.4. Propulsion*

The rocket engines are modelled using standard Tsiolkovsky rocket equations, with configurable inputs specifying the specific impulse $I_{sp}$ and thrust $F_{T_{vac}}$ in a vacuum. A throttle control $\tau \in [0, 1]$ is added that dictates the fraction of maximum available thrust applied and fuel mass flow (and therefore fuel consumption). A simplifying assumption is made that the mass flow varies linearly with thrust. The applied thrust and mass flow rate per engine are then calculated as,

$$\frac{dm_p}{dt} = \dot{m}_p = \tau n_{eng} n_{nozz} \frac{F_{T_{vac}}}{g_0 I_{sp}} \tag{17a}$$

$$F_T(h) = \tau n_{eng} n_{nozz} \left(F_{T_{vac}} - p_{atm}\, A_e\right) \tag{17b}$$

where $n_{nozz}$ are the number of nozzles per engine, and $n_{eng}$ number of engines on the vehicle. A penalty proportional to atmospheric pressure $p_{atm}$ and nozzle exit area $A_e$ is introduced to account for the difference in nozzle expansion under pressure compared to in a vacuum.

The two main stage engines uses a LOX/Kerosene propellant with an $I_{sp}$ between 300-400 s, based on the Yuzhnoye RD-8 series of rocket engines. The number and rating of engines are determined through the design trade-off studies accounting for engine designs currently at TRL 7-9 (i.e., that are either currently available, or predicted to be available in the next 5 years).

### *3.5. Environment*

The Earth is modelled as an oblate spheroid based on the WSG-84 model. The gravitational field was modelled using $4^{\text{th}}$ order spherical harmonics (accounting for $J_2$, $J_3$ and $J_4$ terms) for accelerations in the radial $g_r$ and transverse $g_\phi$ directions.

The atmospheric conditions – temperature $T_{atm}$, pressure $p_{atm}$, density $\rho_{atm}$ and speed of sound – are modelled using the Standard US-76 global static atmospheric model extended up to an altitude of 1000 km above the Earth surface.

### *3.6. Flight dynamics and control*

A 3-DOF variable point mass dynamic model is used where the spaceplane is a time-varying mass located at the centre-of-gravity of the vehicle. The state vector for the flight dynamics $\mathbf{x}_{dyn} = [\mathbf{r},\, \dot{\mathbf{r}}]$ is the spherical coordinates for the position $\mathbf{r} = [r,\, \lambda,\, \theta]$ and the velocity $\dot{\mathbf{r}} = [v,\, \gamma,\, \chi]$ where $r$ is the radial distance, $(\lambda, \theta)$ are the latitude and longitude, $v$ is the magnitude of the relative velocity vector directed by the flight path angle $\gamma$ and the flight heading angle $\chi$. The equations of motion are expressed in the Earth-Centred-Earth-Fixed rotating reference frame (Vinh, 2012; Tewari, 2007).

$$\dot{r} = v \sin\gamma \tag{18a}$$

$$\dot{\lambda} = \frac{v}{r} \cos\gamma \cos\chi \tag{18b}$$

$$\dot{\theta} = \frac{v}{r \cos\lambda} \cos\gamma \sin\chi \tag{18c}$$

$$\dot{v} = \frac{F_T \cos\alpha \cos\mu - D}{m} - g_r \sin\gamma + g_\phi \cos\gamma \cos\chi + \omega_{\mathrm{E}}^2 r \cos\lambda \left(\sin\gamma \cos\lambda - \cos\gamma \cos\chi \sin\lambda\right) \tag{18d}$$

$$\dot{\gamma} = \frac{v}{r} \cos\gamma + \frac{1}{v} \left( \frac{F_T \sin\alpha \cos\mu + L}{m} - g_r \cos\gamma - g_\phi \sin\gamma \cos\chi \right) \tag{18e}$$

$$+ \frac{\omega_E^2 r}{v} \cos\lambda \left(\sin\gamma \cos\chi \sin\lambda + \cos\gamma \cos\lambda\right) + 2\omega_{\mathrm{E}} \sin\chi \cos\lambda \tag{18f}$$

$$\dot{\chi} = \frac{v}{r} \cos\gamma \sin\chi \tan\lambda + \frac{1}{v \cos\gamma} \left( \frac{F_T \sin\mu}{m} - g_\phi \sin\chi \right) \tag{18g}$$

$$+ \omega_{\mathrm{E}}^2 \frac{r \sin\chi \sin\lambda \cos\lambda}{v \cos\gamma} + 2\omega_{\mathrm{E}} \left(\sin\lambda - \tan\gamma \cos\chi \cos\lambda\right) \tag{18h}$$

where $m$ is the time-varying mass of the vehicle, $[g_r,\, g_\phi]$ are the gravitational accelerations in the radial and transverse directions, and $L$ and $D$ are the aerodynamic lift and drag forces, respectively.

The trajectory dynamics are controlled by adjusting the thrust vector. The magnitude of the thrust and mass flow applied is controlled by the

throttle $\tau(t) \in [0,\ 1]$, and the direction through the angle of attack $\alpha(t)$, and the bank angle $\mu(t)$. The engines are assumed fixed with no gimbled thrust at this stage, thus the control law also dictates the partial attitude of the vehicle.

## 4. Optimisation

In this section, the general formulation is presented for trajectory and design optimisation of the conceptual design. The optimisation seeks to find a mission flight profile that minimises the propellant usage, subject to a number of vehicle loading and thermal constraints, and a set of design parameters that both minimise the required gross vehicle mass and maximise the downrange distance while being able to meet the target mission.

The first step was to formulate the problem as an optimal control problem: given the system dynamics for the chosen vehicle configuration, full or partial boundary conditions for the initial and final states of the vehicle and any path constraints, the aim is to find a optimal control law that minimises a given performance index.

The mission is decomposed into a number of user-defined phases, with different system models, objectives and constraints used within each phase (see Fig. 2. The phase decomposition is also used to accommodate discontinuities within the system and performance models, such as separating the sub-, trans- and super/hypersonic aerodynamic models, or for vehicle staging.

A direct multi-shooting transcription method is then employed to transform the continuous optimal control problem into a non-linear programming problem. The NLP is then solved with a local gradient based optimisation algorithm using a multi-start approach to generate first-guess solutions.

### *4.1. Optimal control problem formulation*

Optimal control problems are generally formulated as:

$$\begin{aligned} & \min_{\mathbf{u}\in U} J(\mathbf{x},\mathbf{u},t) \\ s.t.\quad & \dot{\mathbf{x}} = \mathbf{F}(\mathbf{x},\mathbf{u},t) \\ & \mathbf{g}(\mathbf{x},\mathbf{u},t) \geq 0 \\ & \boldsymbol{\psi}(\mathbf{x}_0,\mathbf{x}_f,t_0,t_f) \geq 0 \\ & t \in [t_0,t_f] \end{aligned} \tag{19}$$

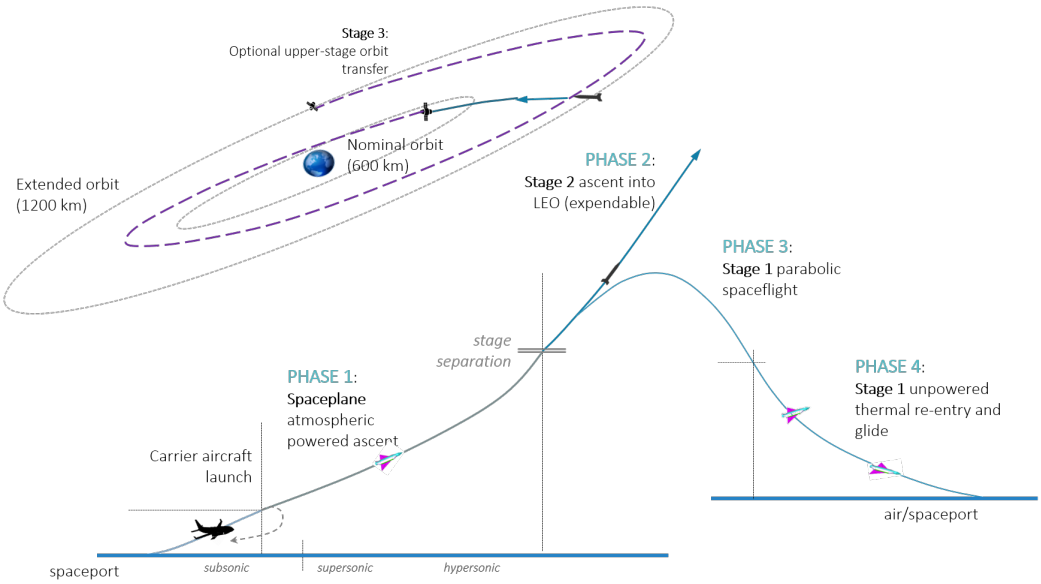


Figure 2: Mission phase decomposition

where $J$ is the objective function of the state vector $\mathbf{x} : [t_0, t_f] \rightarrow \mathbb{R}^n$, control vector $\mathbf{u} \in L^\infty$ and time $t$, $\mathbf{F}$ is a set of differential equations describing the dynamics of the system, $\mathbf{g}$ is a set of algebraic inequalities describing path constraints and $\boldsymbol{\psi}$ is a set of algebraic inequalities describing boundary constraints.

The optimal control problem is transcribed into a nonlinear programming problem by using a multi-phase, multiple-shooting approach. The mission is initially divided into $n_p$ user-defined phases. Within each phase, the time interval is further divided into $n_e$ multiple shooting elements.

$$\cup_{k=1}^{n_p} \cup_{i=0}^{n-1} [t_{i,k}, t_{i+1,k}] \tag{20}$$

The trajectory is numerically integrated for interval $[t_{i,k}, t_{i+1,k}]$ with initial conditions $\mathbf{x}_{i,k}$. Within each interval $[t_{i,k}, t_{i+1,k}]$, the control is further discretised into $n_c$ control nodes $\{u_0^{i,k}, ..., u_{n_c}^{i,k}\}$ and collocated on Tchebycheff points in time.

Continuity constraints on the control and states are imposed between each shooting element, and between phases, matching the state and control vectors at the end of one element, with those at the start of the next.

The trajectory optimisation vector is therefore composed of:

- control nodes within each shooting segment $\{\mathbf{u}_0^{i,k}, ..., \mathbf{u}_{n_c}^{i,k}\}$ for $i = 1, ..., n$ and $k = 1, ..., n_p$,
- time of flight for each shooting segment $\Delta t_k$ for $k = 1, ..., n_p$,
- initial state and control variables of each shooting segment within every phase that should be matched with the previous segment or phase $\mathbf{x}_{1,k}$ and $\mathbf{u}_0^{1,k}$ for $k = 2, ..., n_p$.

In addition, the initial states of the problem can be fixed by the user or left as optimisable parameters. The desired final states are added as boundary constraints to the problem, along with any path constraints evaluated at every integration time step.

### *4.2. Single objective optimisation algorithm*

Problem (19) was solved with the Matlab optimiser `fmincon`, a gradient based local solver for the solution of single objective NLP with nonlinear constraints, using either the interior point or sequential quadratic programming algorithms. The optimisation vector was scaled before the optimisation algorithm such that $\mathbf{u} \in [0, 1]$. The constraints and objective function were also normalised based on user-specified values, typically either the initial or mean value of the optimisation parameter.

A multi-start strategy was used to generate a population of first guess solution vectors within the defined search space. A combination of problem-specific rules, e.g., holding the trajectory controls constant within each element, and assuring an ascending trajectory for the starting state vector of each element, and random sampling through Latin Hypercube Sampling was used to generate a set of first guesses. This allowed a better exploration of the search space and reduces the sensitivity of system to the first guess values while generally allowing for a faster ad higher rate of converge over some stochastic global optimisers.

Integration of the dynamic equations of motion in Eqs. (18) was performed with a fixed step 3$^{\text{rd}}$ order Bogacki-Shampine Runge-Kutta method within the optimisatiaon, and refined, as a post-process, with a variable step Dormand Prince Runge Kutta (4,5) scheme.

### *4.3. Multidisciplinary design optimisation*

A multidisciplinary design optimisation (MDO) approach was used to study the optimality of key design parameters of the vehicle. These design

optimisation parameters were added to the optimisation vector along with the trajectory control parameters given in Section 4.1.

The mission flight path starts just after the separation of the launch vehicle from the carrier aircraft, therefore the initial state vector of the spaceplane is dependant on the state of the carrier aircraft. The altitude and velocity are fixed at a nominal state that could be achieved by the carrier aircraft at separation. A geographic point (latitude and longitude) was selected accounting for range of the carrier aircraft, and safety/regulatory criteria. The flight path and heading angle were left as optimisation design variables, with upper and lower bounds set to allow for the limitations due to the separation manoeuvre.

Static design parameters were added to size the engines for each stage, and the wing area for the returnable, reusable first stage. The overall objective was the minimisation of the gross vehicle mass subject to the nominal design mission which included a target orbit and payload mass, and an unpowered downrange return. This choice of objective required that each of the design choices directly or indirectly affect the mass of the vehicle. The system of parametric mass estimating relationships in Section 3.1 were defined relative to these design variables.

For this study, variations in the mass and sizing of the thermal protection system (TPS) was not included directly in the design optimisation loop, though later studies will examine the requirements for limits on heat load and temperatures based on different TPS.

The propulsion system were sized based on optimising the total mass of propellants for each stage and scaling factors on the maximum vacuum thrust rating for the engines. The mass of the propellant was used to determine the volume and mass of the tanks, while the vacuum rating was used to scale the mass of the engine and engine structure. The engines were scaled relative to two nominal LOX-Kerosene rocket engines manufactured by Yuzhnoye Design Office: the first stage has a main engine with a vacuum thrust of 88.4 tf, vacuum $I_{sp}$ of 332 s and a mass of 1280 kg. The second stage uses the RD-809K engine, with a vacuum thrust of 10 tf, vacuum $I_{sp}$ of 352 s, and a mass of 330 kg.

The sizing of the aerodynamic surfaces is another key design parameter for the vehicle, here through the wing area. As the ascent is rocket-based, with a relatively high thrust force compared to the lift, the ascent drives the design to small wing areas to reduce drag (not accounting for any stability or control surface requirements). The requirement for a glided return to some

coastal site relatively in-plane to the trajectory, drives up the wing area to improve the down or cross ranges achievable. The aerodynamic coefficients for the components are assumed constant for all design options, with the wing reference area $S_{wing}$ scaled relative to the total reference area $S_{ref}$. The lift force $L$ is calculated based on,

$$C_{L,mdo}S_{ref} = C_{L,wing}S_{wing} + C_{L,i}S_i \tag{21}$$

$$L = \frac{1}{2}\rho v_\infty^2 C_{L,mdo}S_{ref} \tag{22}$$

where $C_{L,i}$, $S_i$ are the coefficients of lift and corresponding reference area for the unchanged components of the fuselage, fairing and tail. The wing reference area $S_{wing}$ is scaled relative to the nominal design value. Drag is calculated in the same manner.

In this study, the downrange distance is maximised assuming no cross-range (i.e., the trajectory is entirely in-plane). This is used as a figure of merit for the capabilities of the system assuming no specific landing sites are given, and assuming no requirements for a return to landing site. This is consistent with the commercial drivers for the system that prioritised global operation and flexibility.

## 5. Analysis and results

Two analysis were conducted: the first examines the effect of altering the wing aerodynamics by changing the wing surface area on the vehicle masses and descent performance. The second uses a constant wing surface area and examine the trade-off between mass and engine design with downrange capabilities.

In the following, three different scaling factors for the wing reference area are analysed: 60%, 100% and 120% of $S_{wing}$. The release point was chosen off the west coast of the UK to minimise (or eliminate) the time the atmospheric trajectory was over any populated land. The drop point is determine assuming north-west flight of the carrier aircraft departing from Prestwick airport in Scotland.

The initial state vector $\mathbf{x}(t_0) = [\mathbf{r}, \mathbf{v}]$ is:

$$\mathbf{r}(t_0) = [12 \text{ km}, 58.8058^\circ\text{N}, 12.7471^\circ\text{E}]$$
$$\mathbf{v}(t_0) = [200 \text{ m/s}, \gamma \leq 15^\circ, 0 \leq \chi \leq 90^\circ]$$

The final state vector for Stage 2 ascent to orbit was constrained by the Keplerian orbital parameters: semi-major axis $a = R_E + 650$ km (where $R_E(\lambda)$ is the radius of Earth), eccentricity $e = 0$, inclination $i = 88.2°$. The final state vector for Stage 1 descent was constrained by: altitude $h \leq 1$ km, velocity $v \leq 200$ m/s, and flight path angle $\|\gamma\| \leq 20°$.

Path constraints are added on the normal and axial accelerations such that $|a_x(t)|, |a_z(t)| \leq 4g_0$.

The ascent was optimised based on the objective function,

$$\min_{\mathbf{u}\in\mathbb{D}} (m_{gross}) \tag{24}$$

where the gross vehicle mass is the sum of the dry and fuel masses of Stage 1 and Stage 2, plus the payload mass. The optimisation vector $\mathbf{u}$ contains: the 4 vehicle design variables (vacuum thrust scaling factors for Stage 1 and 2, total fuel mass for Stage 1 and 2), the initial flight path $\gamma_0$ and heading angle $\chi_0$ just after carrier separation, and the trajectory optimisation vector listed in Section 4.1. The user-defined phases of the mission, and the relation to vehicle staging, are shown in Fig. 2.

The atmospheric descent was optimised based on the objective function maximising the central angle of the descent range $d_{gnd}$ based on the start and end points of the atmospheric re-entry phase (Phase 4) and calculated using the Haversine formula.

$$\max_{\mathbf{u}\in\mathbb{D}} \left( \frac{d_{gnd}}{r_{\mathrm{E}}(\lambda = 0)} \right) \tag{25}$$

The re-entry trajectory was broken into 2 phases. The first phase (Phase 3) is the trajectory arc between the separation point of the two stages and the atmospheric re-entry, here defined to start at an altitude of 80 km. In that high altitude phase, the trajectory is ballistic due to the absence of significant atmospheric density and thrust. As such there is no need to derive an optimal control law based on vehicle attitude; this phase was excluded from the optimisation and simply propagated forward in time until the descent altitude reached the set limit. The second phase, Phase 4, is controllable with aerodynamic surfaces, and was thus optimised.

The optimised vehicle design parameters are given in Table 1 based on estimates for a composite material structure. Table 2 gives the optimal initial conditions for the ascent trajectory, and Table 3 reports the optimised values

for the approach to landing of Stage 1, including the maximised downrange distances.

As expected, higher wing areas generally resulted in higher dry masses, propellent masses and engine sizes for each stage. An exception is the second stage for the nominal wing area ($1.0S_{wing}$). While the gross vehicle mass for this case is between the gross masses for the smaller and larger wing areas, as expected, the sizings for each stage differs. The optimiser found a solution with a larger first stage, very similar to that of the $1.2S_{wing}$ case for both engine sizing and mass, and a lighter second stage with a smaller engine. This combination gave the longest downrange distance as a larger first stage means a higher velocity at stage separation, longer ballistic phase and hence better downrange distance. This is also evident from Fig. 5(f) that shows this case has the highest T/W ratio.

Figures 3 and 4 show the optimal trajectories for the nominal wing area. The trajectories are shown for all 4 phases (as illustrated conceptually in Fig. 2). Figure 5 shows the trajectories for the Stage 1+2 combined ascent (Phase 1), followed by the Stage 1 ballistic coast after stage separation (Phase 3), and the Stage 1 atmospheric re-entry (Phase 4) for the 3 different wing areas studied. This shows the trade-off of increasing wing area, where increasing the aerodynamic contribution of wing can increase the glide performance of the vehicle though at the expense of increased dry mass. The net effect shows an optimal configuration somewhere near the nominal wing reference area, looking only at the descent performance.

## 6. Conclusion

This paper presented a conceptual design and performance analysis of a partially re-usable space launch vehicle for small payloads. The system was designed for a nominal mission of delivering a 500 kg payload to a circular 600 km, 88.2° polar orbit. The aim of the system design was to develop a commercially viable launch system for near-term operation, thus emphasis is placed on the efficient use of high TRL technologies. The final design employed a multi-stage, rocket-based spaceplane air-launched from a carrier aircraft. The first stage is fully recoverable through an unpowered glided descent to a secondary landing site. Stage separation occurs around 70 km, with the second expendable stage reaching the nominal mission orbit.

A multidisciplinary design optimisation on the system configuration was run to size the engines of both stages and the Stage 1 wing area. The system

had to meet two objectives: to minimise the gross vehicle mass, and to maximise the downrange. Test cases were run for 3 different wing areas relative to the nominal aerodynamic $S_{wing}$. All test cases are capable of meeting all the mission requirements. The gross masses range between 65–72 tonnes, and the downrange between 716–1343 km. The best downrange was achieved with the nominal wing reference area departing off the coast of Prestwick, with a gross vehicle mass of 70.87 tonnes and a downrange of 1343 km. This configuration had a comparatively larger first stage with an engine vacuum thrust rating of 1164 kN and dry mass of 11343 kg, and a second stage with an engine vacuum thrust rating of 10.6 kN and dry mass of 1852.6 kg.

Table 1: Optimal vehicle design parameters (for a fixed payload mass of 500 kg)

| | Wing area: | $0.6S_{wing}$ | $S_{wing}$ | $1.2S_{wing}$ |
|---|---|---|---|---|
| Stage 1: | Vacuum thrust (kN) | 1112.6 | 1164.3 | 1170.6 |
| | Propellant mass (tonne) | **43.628** | 45.87 | 45.957 |
| | Dry mass (tonne) | **10.665** | 11.343 | 11.635 |
| Stage 2: | Vacuum thrust (kN) | 139.17 | 129.61 | 140.28 |
| | Propellant mass (tonne) | 10.96 | **10.643** | 11.258 |
| | Dry mass (tonne) | 1.8863 | **1.8526** | 1.898 |
| | Vehicle gross mass (tonne) | **68.307** | 70.872 | 71.914 |

Table 2: Optimal initial conditions just after release point from carrier aircraft

| Wing area: | $0.6S_{wing}$ | $S_{wing}$ | $1.2S_{wing}$ |
|---|---|---|---|
| Flight path angle $\gamma(t_0)$ (deg) | 9.47 | 10.81 | 7.06 |
| Flight heading angle $\chi(t_0)$ (deg) | 0.15 | 0.12 | 0.09 |


## Acknowledgements

This work was partially funded by the UK Space Agency through the National Space Technology Programme (NSTP-2) Sub-Orbital and Small Launcher Research Projects Call, and the European Space Agency through General Support Technology Programme (GSTP).

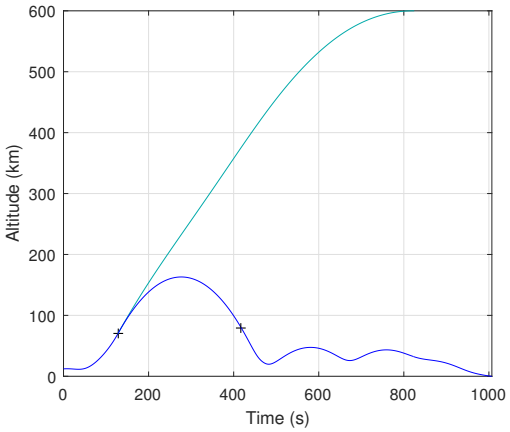


(a) Altitude

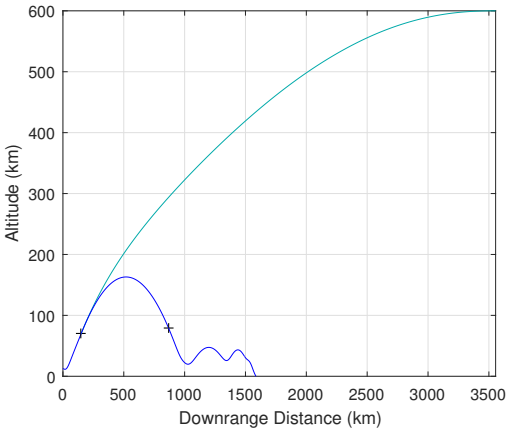


(b) Altitude vs groundtrack

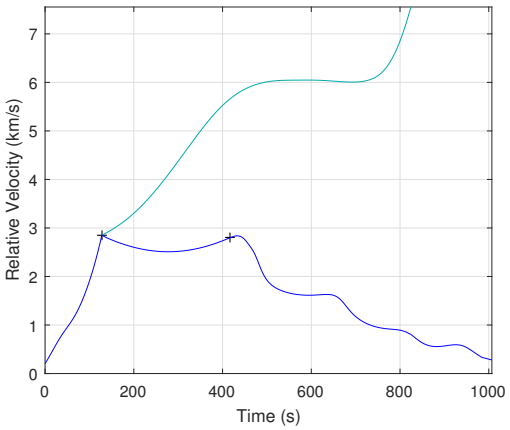


(c) Velocity

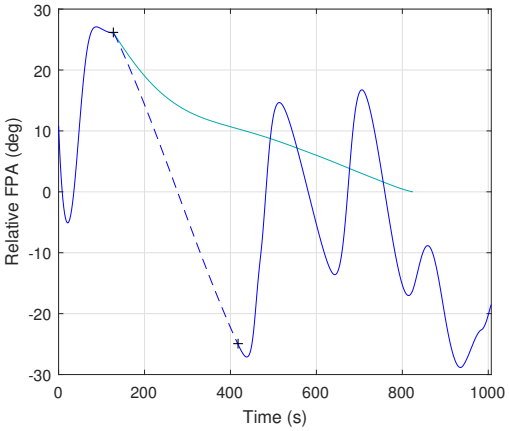


(d) Flight path angle

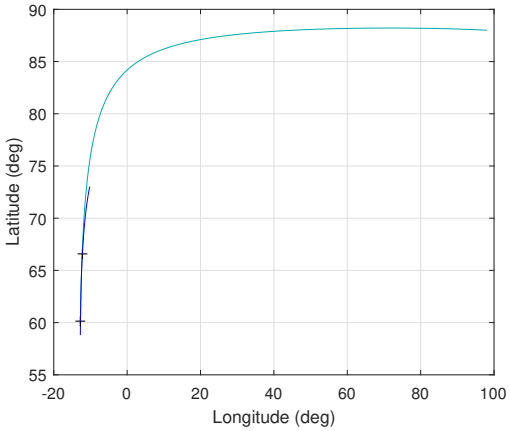


(e) Latitude vs longitude

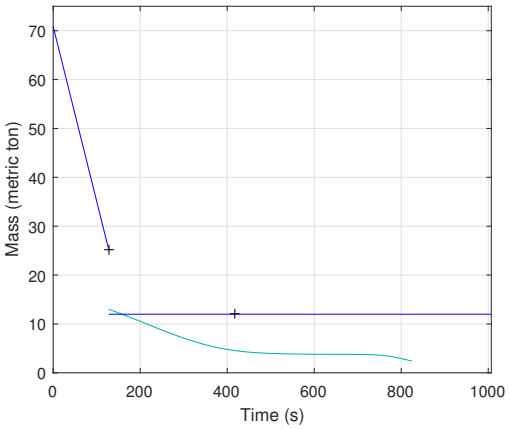


(f) Vehicle mass

Figure 3: Trajectory results for reference case, $1.0S_{wing}$. Start/end of phases are indicated by crosses.

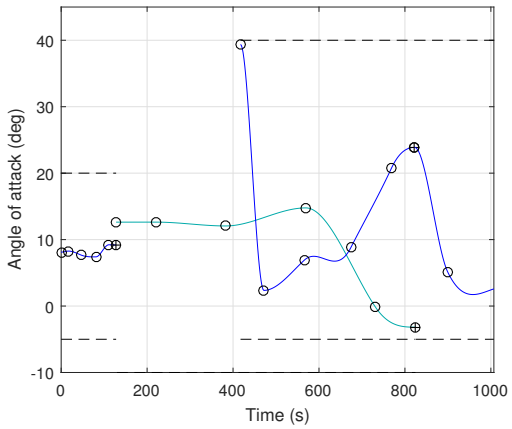


(a) Angle of attack

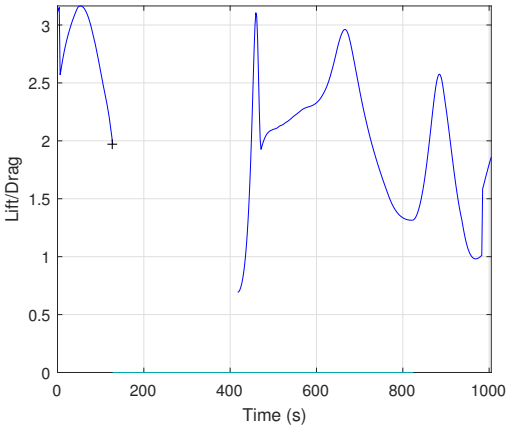


(b) Lift-to-drag ratio

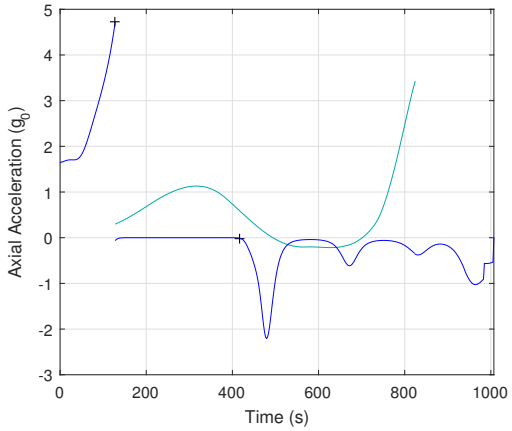


(c) Axial acceleration

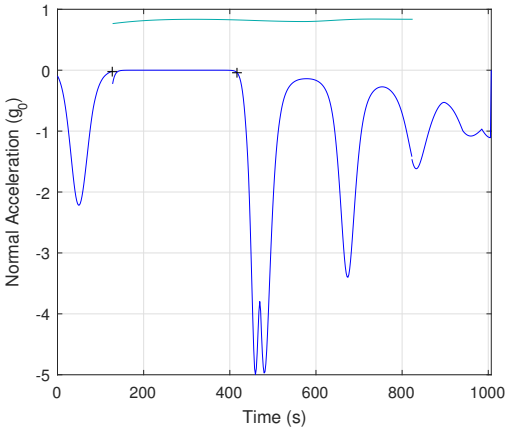


(d) Normal acceleration

Figure 4: Control laws, forces and accelerations for reference case, $1.0S_{wing}$. Start/end of phases are indicated by crosses.

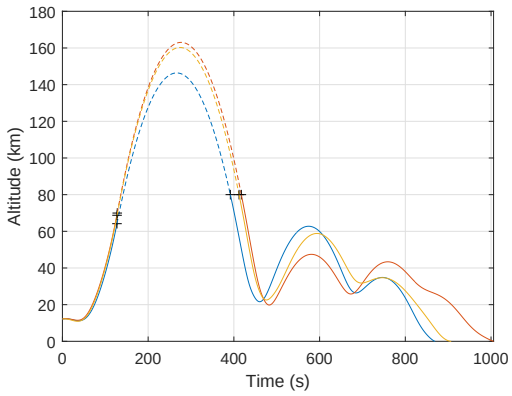


(a) Altitude over time

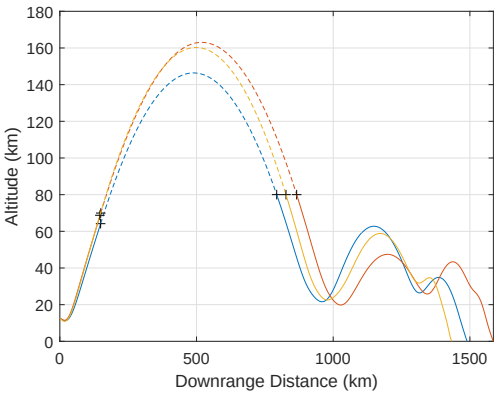


(b) Altitude against groundtrack

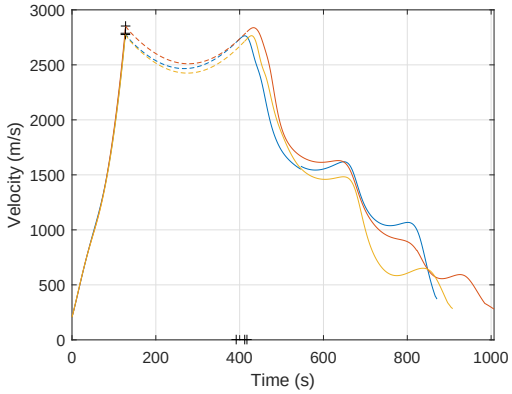


(c) Velocity

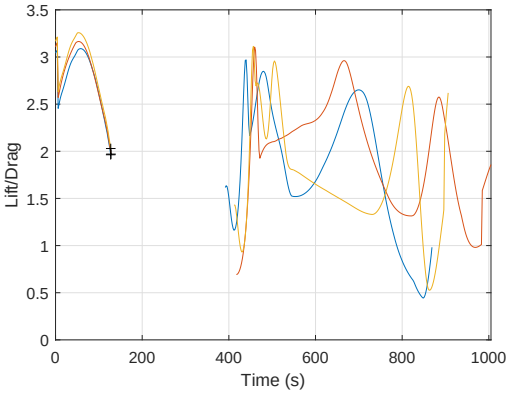


(d) Lift-to-drag ratio

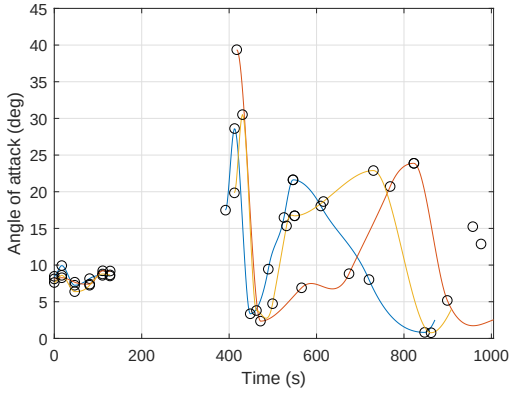


(e) Angle of attack

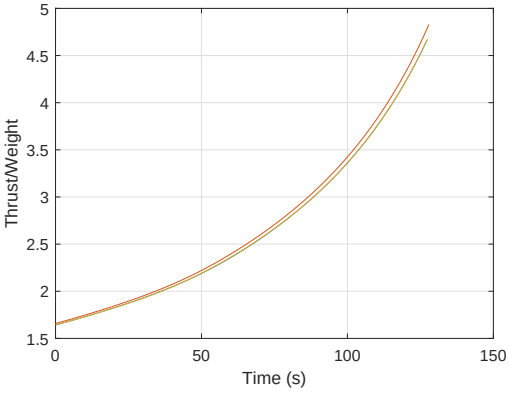


(f) Thrust-to-weight ratio

Figure 5: Comparison of trajectory and design parameters for different wing surface areas: $0.6S_{wing}$ (blue), $1.0S_{wing}$ (red), and $1.2S_{wing}$ (orange). Dashed lines indicate ballistic spaceflight segments.

Table 3: Final spaceport approach conditions

| Wing area: | $0.6S_{wing}$ | $S_{wing}$ | $1.2S_{wing}$ |
|---|---|---|---|
| Altitude $h$ (m) | 928 | 442 | 503 |
| Velocity $v$ (m/s) | 265 | 294 | 328 |
| Mach | 0.788 | 0.87 | 0.97 |
| Flight path angle $\gamma$ (deg) | -14.00 | -19.95 | -18.19 |
| Downrange distance (km) | 1332 | **1343** | 961 |

## References


Detra, R., 1961. Generalized heat transfer formulas and graphs for nose cone re-entry into the atmosphere. ARS Journal 31 (3), 318–321.

Doncaster, B., Williams, C., Shulman, J., 2017. 2017 nano/microsatellite market forecast. Tech. rep., PricewaterhouseCoopers.

Fleeman, E., 2001. Tactical missile design. AIAA Education Series.

Hay, J., Guthrie, P., Mullins, C., Gresham, E., Christensen, C., 2009. Global space industry: Refining the definition of new space. In: AIAA SPACE 2009 Conference & Exposition.

Jorgensen, L. H., 1973. A method for estimating static aerodynamic characteristics for slender bodies of circular and noncircular cross section alone and with lifting surfaces at angles of attack from 0° to 90°. Tech. Rep. NASA TN D-7228.

MacConochie, I. O., Lepsch Jr, R. A., 2002. Characterization of subsystems for a WB-003 single stage shuttle. Tech. Rep. NASA/CR-2002-211249.

Maddock, C., Kontis, K., McIntyre, S., West, M., Feast, S., Evans, D., 2016a. How to launch small payloads? evaluation of current and future small payload launch systems. In: Reinventing Space Conference.

Maddock, C., Toso, F., Ricciardi, L., Mogavero, A., Lo, K., Rengarajan, S., Kontis, K., Milne, A., Merrifield, J., Evans, D., West, M., McIntyre, S., 2017. Vehicle and mission design of a future small payload launcher. In: 21st AIAA International Space Planes and Hypersonics Technologies Conference.

601 Maddock, C., West, M., Kontis, K., Feast, S., Evans, D., McIntyre, S., 2016b.
602 A commercially driven design approach to uk future small payload launch
603 systems. In: Reinventing Space Conference.

604 Mason, L. A., Devan, L., Moore, F. G., McMillan, D., 1981. Aerodynamic
605 design manual for tactical weapons. Tech. rep., DTIC Document.

606 Rohrschneider, R., 2002. Development of a mass estimating relationship
607 database for launch vehicle conceptual design. AE8900 Special Project,
608 School of Aerospace Engineering, Georgia Institute of Technology.

609 SAE AC-9, 1969. SAE Aerospace Committee on Aircraft Environmental Sys-
610 tems: Applied Thermodynamics Manual.

611 Schaaf, S. A., 1964. Heat transfer in rarefied gases. In: Rohsenow, W. M.
612 (Ed.), Developments in heat transfer. MIT Press, Ch. 7.

613 Singh, A., 1996. Experimental study of slender vehicles at hypersonic speeds.
614 Ph.D. thesis, Cranfield University.

615 Tewari, A., 2007. Atmospheric and space flight dynamics. Springer.

616 Vinh, N., 2012. Optimal trajectories in atmospheric flight. Vol. 2. Elsevier.